

Article

# A Significant Solar Energy Note on Powell-Eyring Nanofluid with Thermal Jump Conditions: Implementing Cattaneo-Christov Heat Flux Model

Nidal H. Abu-Hamdeh <sup>1</sup>, Radi A. Alsulami <sup>2</sup>, Muhyaddin J. H. Rawa <sup>3</sup>, Mashhour A. Alazwari <sup>2</sup>,  
Marjan Goodarzi <sup>4,5</sup> and Mohammad Reza Safaei <sup>6,7,\*</sup>

- <sup>1</sup> Center of Research Excellence in Renewable Energy and Power Systems, and Department of Mechanical Engineering, Faculty of Engineering, King Abdulaziz University, Jeddah 21589, Saudi Arabia; nabuhamdeh@kau.edu.sa
  - <sup>2</sup> Mechanical Engineering Department, Faculty of Engineering, King Abdulaziz University, Jeddah 21511, Saudi Arabia; rasalsulami@kau.edu.sa (R.A.A.); maalazwari@kau.edu.sa (M.A.A.)
  - <sup>3</sup> Center of Research Excellence in Renewable Energy and Power Systems, Department of Electrical and Computer Engineering, Faculty of Engineering, King Abdulaziz University, Jeddah 21589, Saudi Arabia; mrawa@kau.edu.sa
  - <sup>4</sup> Mechanical Engineering Department, Lamar University, Beaumont, TX 77706, USA; mgoodarzi@lamar.edu
  - <sup>5</sup> Department of Mathematics, Faculty of Science, King Abdulaziz University, P.O. Box 21521, Jeddah, Saudi Arabia
  - <sup>6</sup> Department of Mechanical Engineering, Florida International University, Miami, FL 33174, USA
  - <sup>7</sup> Department of Medical Research, China Medical University Hospital, China Medical University, Taichung 40402, Taiwan
- \* Correspondence: cfd\_safaei@fiu.edu; Tel.: +1-502-657-9981



**Citation:** Abu-Hamdeh, N.H.; Alsulami, R.A.; Rawa, M.J.H.; Alazwari, M.A.; Goodarzi, M.; Safaei, M.R. A Significant Solar Energy Note on Powell-Eyring Nanofluid with Thermal Jump Conditions: Implementing Cattaneo-Christov Heat Flux Model. *Mathematics* **2021**, *9*, 2669. <https://doi.org/10.3390/math9212669>

Academic Editor: James M. Buick

Received: 22 September 2021

Accepted: 18 October 2021

Published: 21 October 2021

**Publisher's Note:** MDPI stays neutral with regard to jurisdictional claims in published maps and institutional affiliations.



**Copyright:** © 2021 by the authors. Licensee MDPI, Basel, Switzerland. This article is an open access article distributed under the terms and conditions of the Creative Commons Attribution (CC BY) license (<https://creativecommons.org/licenses/by/4.0/>).

**Abstract:** PTSCs (parabolic trough solar collectors) are widely employed in solar-thermal applications to attain high temperatures. The purpose of this study is to determine how much entropy is created when Powell-Eyring nanofluid (P-ENF) flows across porous media on a horizontal plane under thermal jump circumstances. The flow in PTSC was generated by nonlinear surface stretching, thermal radiation, and Cattaneo-Christov heat flux, which was utilized to compute heat flux in the thermal boundary layer. Using a similarity transformation approach, partial differential equations were converted into ordinary differential equations with boundary constraints. Then, the boundary restrictions and partial differential equations were merged to form a single set of nonlinear ordinary differential equations. To obtain approximate solutions to ordinary differential equations, the Keller-Box approach is utilized. Nanofluids derived from silver- and copper-based engine oil (EO) has been employed as working fluids. The researchers observed that changing the permeability parameter reduced the Nusselt number while increasing the skin frictional coefficient. Total entropy variation was also calculated using the Brinkman number for flow rates with Reynolds number and viscosity changes. The key result is that thermal efficiency is inversely proportional to particular entropy production. For example, using Cu-EO nanofluid instead of Ag-EO nanofluid increased the heat transport rate efficiency to 15–36%.

**Keywords:** parabolic trough solar collector; P-ENF; Cattaneo-Christov heat flux; entropy generation; Keller-box method

## 1. Introduction

It can be said that renewable energy is vital for humankind's future because all aspects of advanced humans depend on energy. This is an inseparable section of industry, transport, building consumptions, and so on. So far, accelerated developments cause fossil fuels, which are the main sources of energy, to evacuate. For this reason, scientists worldwide have embarked on finding alternative resources. For example, solar energy, an energy source from early man, is now used in macroscale plans. Plus, the renewability of solar

energy is clean, and not having any emissions is one of its advantages against what is known as global warming nowadays, which is induced from burning fossil fuels.

Parabolic trough solar collectors (PTSCs) are a technology that has the most application in solar harnessing. Thermal analysis of this system has attracted attention for obtaining an optimum working condition to achieve higher proficiency of power plants [1,2]. One practical suggestion is nanotechnology in PTSC systems. Nanoparticles have a high ability to ameliorate thermal efficiency when dispersing through a base fluid to form nanofluids [3]. Heretofore, extended studies have widely proved that the superior characteristics of nanofluids are a helpful approach to achieve high transferring phenomena [4]. Nanoparticles act as an excellent energy carrier through fluids. Hence, the thermal conductivity of nanofluids is generally better than conventional fluids. This leads to a higher heat transfer coefficient and Nusselt number in a typical thermal system [5]. However, adding nanoparticles to the base fluid may change the base fluid's rheological behavior, i.e., non-Newtonian behavior appears in some nanofluids [6,7].

Fluids with complicated rheological behavior such as grease, paints, blood, some oils, polymers, nanofluids, and nano-lubricants are not easy to be predicted by conventional equations. Non-Newtonian models are well-known as Casson, power law, Reiner-Philippoff, Carreau, micropolar, Prandtl-Eyring, Prandtl, and Powell-Eyring have wide application in industrial and practical situations [8]. Powell-Eyring fluid was firstly modeled and introduced by Powell and Eyring [9]. However, until now, many developments have been presented. Scientists are concerned that kinetic theory is the main reason for Powell-Eyring fluids' dynamic existence rather than their realistic explanation [10]. Hayat et al. [11] claimed that the Powell-Eyring model has the ability to decrease the viscous property of this kind of fluid to a mobile ambulatory surface at any power of shear concentration. The Powell-Eyring model suitably approximates the timely rheological behavior of the fluid. Jamshed et al. [12] studied Maxwell nanofluid constructed by Cu and TiO<sub>2</sub> in CH<sub>3</sub>OH through a PTSC. The Keller-Box was the method of salvation. Higher thermal performance was observed by Cu/ CH<sub>3</sub>OH nanofluid that was 29%. Cu-MoS<sub>2</sub>/EO nanofluid flow with Reiner Philippoff behavior was verified by Sajid et al. [13] in a PTSC. The nanofluid concentration led to entropy generation enhancement. Furthermore, parameters corresponding to penetrability and heat generation had the same effect. Al-Rashed et al. [14] modeled a PTSC system that worked with non-Newtonian water-CMC-based nanofluid. They found that 100 nm Al<sub>2</sub>O<sub>3</sub> nanoparticles with a 1.5% volume fraction in base fluid have the ability to increase the system's performance by almost 62% with an insulation angle of 90°. Mwesigye et al. [15] reported that a 2.5 vol.% of SWCNT nanoparticles within Therminol can augment the heat transfer by 234% and dwindle the entropy generation by 70%. At the same time, it enhances the thermal efficiency by only 4.4%. Siavashi et al. [16] examined the effect of nanofluid and porous media in a PTSC. Findings indicated that 0.015 vol.% of Cu can improve the Nusselt number and thermal efficiency by 12% and 1.2%, respectively. However, using porous media enhanced the Nusselt number by 10 times more than without porosity. Xiong et al. [17] investigated power-law nanofluid containing Cu nanoparticles through PTSC. At shear-thinning rheological behavior, rising nanofluid concentration had a remarkable enhancement effect on the Nusselt number. In contrast, it had no perceptible change in shear-thickening state. Ebrahimi-Moghadam et al. [18] conducted an optimization study to minimize entropy through a PTSC system that uses Al<sub>2</sub>O<sub>3</sub>/EG-water nanofluid. Rising nanofluid concentration augmented the entropy generation and its thermal parameter, in contrast to frictional entropy generation. Yan et al. [19] numerically surveyed non-Newtonian Fe<sub>3</sub>O<sub>4</sub>-CNT/water-CMC nanofluid flow in PTSC. They reported that the thermal performance of a dual-pass tube, in all cases, is higher than a single one. Besides, the higher the nanofluid concentration, the higher the efficiency. Chaudhari et al. [20] experimentally indicated that adding 0.1 vol.% Al<sub>2</sub>O<sub>3</sub> nanoparticles to water can improve the thermal efficiency and heat transfer coefficient by up to 0.7% and 32%. Okonkwo et al. [21] carried out entropy generation optimization of SiO<sub>2</sub>/water nanofluid through the PTSC system. They used machine learning (ANN method) to predict

the entropy rate. They also investigated the Green-Synthesized  $\text{TiO}_2$ /water entropy rate in PTSC in [22]. In this study, they observed that the Nusselt number and entropy generation fall by increasing nanofluid concentration; however, nanofluid's heat convection was higher than distilled water.

Furthermore, nanofluid amended the thermal efficiency of the PTSC system. In a comprehensive survey, Hachicha et al. [23] experimentally and numerically scrutinized the influence of MWCNT/water nanofluid in a PTSC. The experiments illustrated that adding 0.3 vol.% nanoparticles triggers a 21% enhancement in the Nusselt number. On the other hand, the entropy generation decreased by increasing the concentration while increasing the Reynolds number had no regressive effect on thermal entropy. Hence, they concluded that using nanofluid should be considered at low Reynolds numbers. Hosseini and Shafiey Dehaj experimentally explored the role of GO/water nanofluid and  $\text{Al}_2\text{O}_3$ /water nanofluid in PTSC. GO/water had a 63.2% thermal performance enhancement, about two times greater than another nanofluid. Entropy generation at the presence of Cattaneo-Christov heat flux in PTSC system under the influence of Cu-ZrO<sub>2</sub>/EG nanofluid determined by Jamshed et al. [24]. Keller-Box was used as the modeling method. It was revealed that skin fractional was closely related to porous media, and the slip parameter quenched the Nusselt number. In contrast, skin fractional decreased the Nusselt number.

Due to solar systems' wide practical and industrial application, it is crucial to search in entropy and thermal efficiency in this area. Besides, the role of nanofluids in PTSCs and their behavior need to be determined further. As checked prior, a detailed study of using P-ENF fluid around a heated surface taking into account the Cattaneo-Christov model through PTSC has not been interrogated. Three main aspects covered the inspiration for this research. First, two different nanofluids containing Cu and Ag nanoparticles dispersed in ethylene glycol were considered to pursue the Powell-Eyring nanofluid. Second, the Cattaneo-Christov model was supposed to be the heat flux approach. Third, the raised non-linear ODE equations were solved by the Keller-Box scheme. Exciting results emphasized that the permeability parameter affects the Nusselt number and skin friction coefficient. Furthermore, total entropy as a function of the Brinkman number was scrutinized by changing the Reynolds number and viscosity. It was found that particular entropy production and thermal efficiency have an inverse relation. Finally, Cu-EG nanofluid showed a remarkable enhancement in the efficiency of the rate of heat transport up to 36%.

## 2. Mathematical Formulation

The model with the non-uniform stretching velocity describes the moving flat solid surface [25]:

$$U_w(x, 0) = bx \quad (1)$$

Here,  $b$  is the primary stretching ratio. The temperature of the insulated sheet is  $\Upsilon_w(x, 0) = \Upsilon_\infty + b^*x$  and for ease of performance, it is considered to be firmed at  $x = 0$ ,  $b^*$ ,  $\Upsilon_w$  and  $\Upsilon_\infty$ . For the stands, temperature variation rate, wall temperature, and its nearby. The surface is presumed to possess a slip effect, and the sheet is subjected to a temperature gradient. The 2-dimensional incompressible steady flow, boundary-layer approximations, phase flow model, and the non-Newtonian P-ENF are considered. The different efforts are also considered i.e., porous medium, thermal radiative flow, Cattaneo-Christov heat flux, viscous dissipation, eat source and porous stretching surface, and convection and slippery boundary constraints. The internal geometry of the PTSC is illustrated in Figure 1.

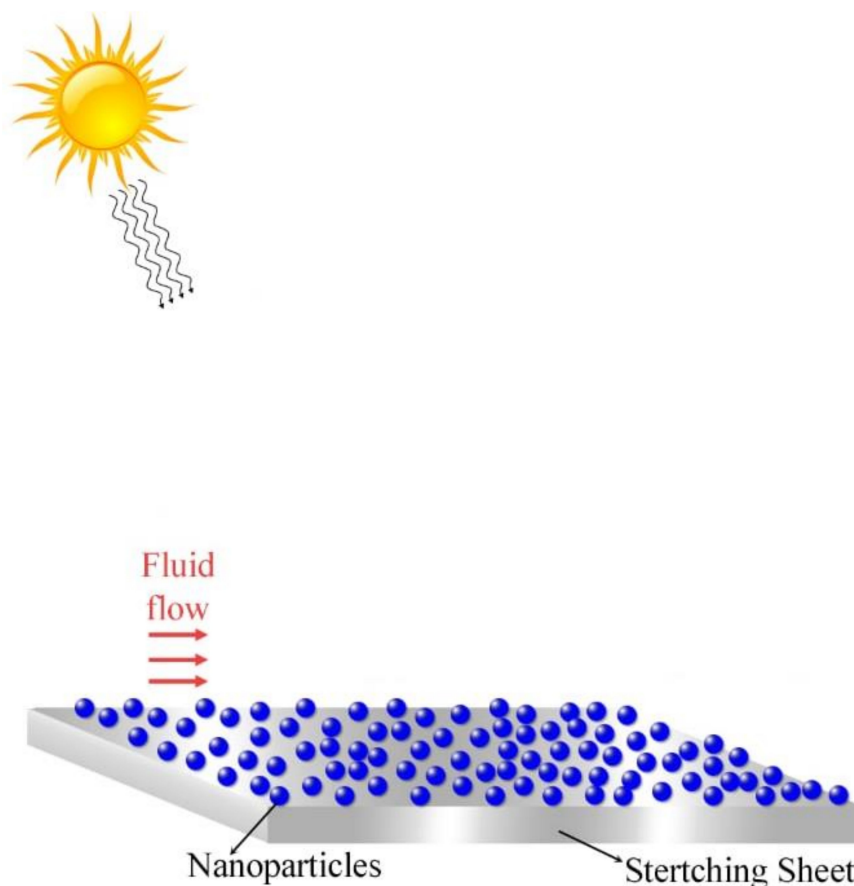


Figure 1. Schematic of the flow model.

The modeling equations for conserved mass, flow, and thermal equations were considered as in Ref. [26] modified with boundary layer claims adopted for 2-D, steady flow conditions of Powell-Eyring nanofluid (P-ENF) along with porous medium, heat source, radiation heat flux, and Cattaneo-Christov heat flux are [26–28]:

$$\frac{\partial E_1}{\partial x} + \frac{\partial E_2}{\partial y} = 0, \tag{2}$$

$$E_1 \frac{\partial E_1}{\partial x} + w_2 \frac{\partial E_1}{\partial y} = \left( v_{nf} + \frac{1}{\rho_{nf} \tilde{\beta} \zeta^*} \right) \left( \frac{\partial^2 E_1}{\partial y^2} \right) - \frac{1}{2 \tilde{\beta} \zeta^{*3} \rho_{nf}} \frac{\partial^2 E_1}{\partial y^2} \left[ \left( \frac{\partial E_1}{\partial y} \right)^2 \right] - \frac{\mu_{nf}}{\rho_{nf} k} E_1, \tag{3}$$

$$E_1 \frac{\partial \Upsilon}{\partial x} + E_2 \frac{\partial \Upsilon}{\partial y} = \frac{k_{nf}}{(\rho C_p)_{nf}} \left[ \frac{\partial^2 \Upsilon}{\partial y^2} \right] + \frac{1}{(\rho C_p)_{nf}} Q_\epsilon [\Upsilon - \Upsilon_\infty] + \frac{\mu_{nf}}{(\rho C_p)_{nf}} \left[ \frac{\partial E_1}{\partial y} \right]^2 - \frac{1}{(\rho C_p)_{nf}} \left[ \frac{\partial q_r}{\partial y} \right] - \Upsilon \left[ E_1 \frac{\partial E_1}{\partial x} \frac{\partial \Upsilon}{\partial x} + E_2 \frac{\partial E_2}{\partial y} \frac{\partial \Upsilon}{\partial y} + E_1 \frac{\partial E_2}{\partial x} \frac{\partial \Upsilon}{\partial y} + E_2 \frac{\partial E_1}{\partial y} \frac{\partial \Upsilon}{\partial x} + E_1^2 \frac{\partial^2 \Upsilon}{\partial x^2} + E_2^2 \frac{\partial^2 \Upsilon}{\partial y^2} + 2 E_1 E_2 \frac{\partial^2 \Upsilon}{\partial x \partial y} \right]. \tag{4}$$

The relevant boundary conditions are [28]:

$$E_1(x, 0) = U_w + N_L \left( \frac{\partial E_1}{\partial y} \right), \quad v_2(x, 0) = V_L, \quad -k_L \left( \frac{\partial \Upsilon}{\partial y} \right) = h_L (\Upsilon_w - \Upsilon), \tag{5}$$

$$E_1 \rightarrow 0, \quad \Upsilon \rightarrow \Upsilon_\infty \text{ as } y \rightarrow \infty. \tag{6}$$

Flow velocity holds in the form as  $\vec{E} = [E_1(x, y), E_2(x, y), 0]$ .  $\tilde{\beta}$  and  $\zeta^*$  are material constants,  $\Upsilon$  is fluid temperature. The fluid relaxation and thermal relaxation factors are expressed as  $\lambda$  and  $Y$ , respectively. Other crucial parameters are surface permeability  $V_L$ , heat source ( $Q_\epsilon$ ), slip length ( $N_L$ ) heat transfer coefficient  $h_L$ , porosity ( $k$ ) and heat conductivity of firm  $k_L$ . Physical features identical, the convective animated surface

experienced its heat loss through conductive (Newtonian thermal) and flowing swiftness close to the sheet, which is comparative to the cut stress exerts in it (slippy form) are deliberate. Table 1 summarizes the material specifications for the P-ENF nanofluid [29,30].

**Table 1.** Thermophysical properties for Powell-Eyring Nanofluid [29,30].

Features	Nanoliquid
Dynamical viscidness ( $\mu$ )	$\mu_{nf} = \mu_f(1 - \phi)^{-2.5}$
Density ( $\rho$ )	$\rho_{nf} = (1 - \phi)\rho_f - \phi\rho_s$
Heat capacity ( $\rho C_p$ )	$(\rho C_p)_{nf} = (1 - \phi)(\rho C_p)_f - \phi(\rho C_p)_s$
Thermal conductivity ( $\kappa$ )	$\frac{\kappa_{nf}}{\kappa_f} = \left[ \frac{(\kappa_s + 2\kappa_f) - 2\phi(\kappa_f - \kappa_s)}{(\kappa_s + 2\kappa_f) + \phi(\kappa_f - \kappa_s)} \right]$

In Table 1, ( $\phi$ ) is nanoparticle fractional volume,  $\rho_f$  and  $\rho_s$  are fluid and particle density values,  $\mu_f$  is dynamic viscosity,  $(C_p)_f$  and  $(C_p)_s$  are heat capacity values of fluid and particle,  $\kappa_f$  and  $\kappa_s$  are thermal conductivities of fluid and particles. As the thickness of the non-Newtonian P-ENF restricts the radiation to pass through extend, the Rosseland approximation [31] is adopted to model the radiation correctly:

$$q_r = -\frac{4\sigma^*}{3k^*} \frac{\partial \Psi^4}{\partial y}. \tag{7}$$

In Equation (7),  $k^*$  stands for the absorption coefficient,  $\sigma^*$  describes Stefan Boltzmann number. Material properties of the engine oil, Cu, and Ag nanoparticles are shown in Table 2 [32–34].

**Table 2.** Material specifications at 20 °C [32–34].

Thermophysical	$\rho$ (kg/m <sup>3</sup> )	$c_p$ (J/kgK)	$k$ (W/mK)
Copper (Cu)	8933	385.0	401.00
Engine Oil (EO)	884	1910	0.144
Silver (Ag)	10500	235	429

### 3. Dimensionless Formulations Model

The crucial step of solving this BVP Equations (2)–(4) is to handle the PDEs. By engaging the similarity variables, it has been done smoothly and converted to simplified ODEs. Stream functions can be given as [28]:

$$E_1 = \frac{\partial \psi}{\partial y}, \quad E_2 = -\frac{\partial \psi}{\partial x}. \tag{8}$$

and similarity variables as [25]:

$$\omega(x, y) = \sqrt{\frac{b}{v_f}} y, \quad \psi(x, y) = \sqrt{v_f b x} f(\omega), \quad \theta(\omega) = \frac{\Psi - \Psi_\infty}{\Psi_w - \Psi_\infty}. \tag{9}$$

into Equations (2)–(4). We get

$$\left( \frac{1}{\phi_1 \phi_2} + \frac{\bar{\omega}_2}{\phi_1} \right) f'''' + f f'' - f'^2 - \frac{\bar{\omega}_1 \bar{\omega}_2}{\phi_2} f'^2 f'''' - \frac{1}{\phi_1 \phi_2} K_\epsilon f' = 0, \tag{10}$$

$$\theta'' \left( 1 + \frac{1}{\phi_4} P_r N_\epsilon \right) + P_r \frac{\phi_3}{\phi_4} \left[ f \theta' - f' \theta + \theta \frac{Q_\epsilon}{\phi_3} + \frac{E_\epsilon}{\phi_1 \phi_3} f'^2 - Y_\epsilon (f'^2 \theta - f'' \theta - f^2 \theta^2 - f f' \theta'') \right] = 0. \tag{11}$$

with 
$$\left. \begin{aligned} f(0) = S, & \quad f'(0) = 1 + \Lambda_\epsilon f''(0), \theta'(0) = -B_\gamma(1 - \theta(0)) \\ f'(\omega) \rightarrow 0, & \quad \theta(\omega) \rightarrow 0, \text{ as } \zeta \rightarrow \infty \end{aligned} \right\} \quad (12)$$

where  $\phi_i$ 's is  $1 \leq i \leq 4$  in formulas (10), (11) signify the subsequent thermo-physical structures for P-ENF [26]

$$\left. \begin{aligned} \phi_1 &= (1 - \phi)^{2.5}, \quad \phi_2 = \left(1 - \phi + \phi \frac{\rho_s}{\rho_f}\right), \quad \phi_3 = \left(1 - \phi + \phi \frac{(\rho C_p)_s}{(\rho C_p)_f}\right) \\ \phi_4 &= \left(\frac{(k_s + 2k_f) - 2\phi(k_f - k_s)}{(k_s + 2k_f) + \phi(k_f - k_s)}\right). \end{aligned} \right\} \quad (13)$$

As Equation (2) is satisfied identically, the notation (') represents the derivatives concerning  $\omega$ . Here,  $\bar{\omega}_1 = \frac{U_w^2}{2\zeta^2 v_f x}$  (non-Newtonian Powell-Eyring parameter-I),  $\bar{\omega}_2 = \frac{1}{\mu_f \beta \zeta^*}$  (non-Newtonian Powell-Eyring parameter-II), and  $K_\epsilon = \frac{v_f}{bk}$  (porous medium) parameters defined along with  $Y = b\lambda_0$  (relaxation time),  $Pr = \frac{v_f}{\alpha_f}$  (Prandtl number),  $\alpha_f = \frac{k_f}{(\rho C_p)_f}$  (thermal diffusivity),  $S = -V_L \sqrt{\frac{1}{v_f b}}$  (mass transfer),  $Q_\epsilon = \frac{Q_0}{(\rho C_p)_f b}$  (heat source),  $N_\epsilon = \frac{16}{3} \frac{\sigma^* \zeta_\infty^3}{\kappa^* v_f (\rho C_p)_f}$  (thermal radiation),  $\Lambda_\epsilon = \sqrt{\frac{b}{v_f}} N_L$  (velocity slip),  $E_\epsilon = \frac{U_w^2}{(C_p)_f (T_w - T_\infty)}$  (Eckert number) and  $B_\gamma = \frac{h_L}{k_L} \sqrt{\frac{v_f}{b}}$  (Biot number) parameters, respectively.

Other two physically vital parameters like skin level friction ( $C_f$ ) and the reduced Nusselt number ( $Nu_x$ ) can be expressed as [26]:

$$C_f Re_x^{\frac{1}{2}} = \left[ \left( \frac{1}{(1 - \phi)^{2.5}} + \bar{\omega}_2 \right) f''(0) - \frac{\bar{\omega}_1 \bar{\omega}_2}{3} (f''(0))^3 \right], \quad Nu_x Re_x^{-\frac{1}{2}} = -\frac{k_{nf}}{k_f} (1 + N_\epsilon) \theta'(0), \quad (14)$$

where  $Re_x = \frac{U_w x}{v_f}$  is the local Reynolds number.

#### 4. Computational Procedure: KBM

The set of nonlinear ODE's (11), (12), resulting from nanofluid flow mathematical modeling, is analytically strenuous to overcome. However, owing to its rapid convergence, the Keller-Box approach (KBM) [35] is employed to solve the model formulas (Figure 2). This approach is typically frequently used in the study of laminar boundary layer flow. The procedure of KBM is as follows:

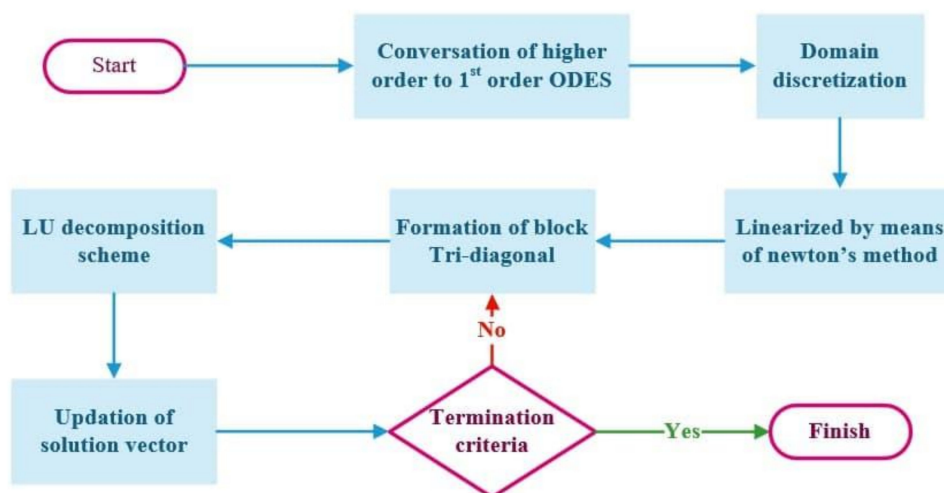


Figure 2. Chart of KBM steps.

All of the ODEs should be transformed into 1st-order ODEs, in initial stages (10)–(12)

$$P_1 = f', \tag{15}$$

$$P_2 = v_1' P_2 = v_1', \tag{16}$$

$$P_3 = \theta', \tag{17}$$

$$\left(\frac{1}{\phi_1 \phi_2} + \frac{\bar{\omega}_2}{\phi_1}\right) P_2' + f P_2 - P_1^2 - \frac{\bar{\omega}_1 \bar{\omega}_2}{\phi_2} P_2^2 P_2' - \frac{1}{\phi_1 \phi_2} K_\epsilon P_1 = 0, \tag{18}$$

$$P_3' \left(1 + \frac{1}{\phi_4} P_r N_\epsilon\right) + P_r \frac{\phi_3}{\phi_4} \left[ f P_3 - P_1 \theta + \theta \frac{Q}{\phi_3} + \frac{E_\epsilon}{\phi_1 \phi_3} P_2^2 - Y_\epsilon \left( P_1^2 \theta - P_2 \theta - f^2 \theta^2 - f P_1 P_3' \right) \right] = 0. \tag{19}$$

Presence of newly variables, boundary conditions eventually turn [36]:

$$f(0) = S, P_1(0) = 1 + \Lambda_\epsilon P_2(0), P_3(0) = -B_\gamma (1 - \theta(0)), P_1(\infty) \rightarrow 0, \theta(\infty) \rightarrow 0. \tag{20}$$

### 5. Code Validation

The validation of the present numerical solution was measured by comparing the heat transfer rate from the current method with the outcomes of a former study [37] through Table 3. As can be seen, the outcomes of the present analysis are in agreement with the former study.

**Table 3.** Comparing  $-\theta'(0)$  with alteration in Prandtl number, and taking  $\phi = 0, \gamma = 0, \Lambda_\epsilon = 0, N_\epsilon = 0, B_\gamma = 0, Q_\epsilon = 0, E_\epsilon = 0$  and  $S = 0$ .

$P_r$	Rana & Nawaz [37]	This Study
0.72	0.74454088	0.8087618
1.0	0.91192959	1.0000000
3.0	1.81548127	1.9235742
7.0	2.96744744	3.0731465
10	3.61534147	3.7205542

### 6. Analysis of Entropy Generation

Porous media generally increase the entropy of the system. For example, Das et al. [38] described the nanofluid entropy production by:

$$E_G = \frac{k_{nf}}{\Upsilon_\infty^2} \left\{ \left( \frac{\partial \Upsilon}{\partial y} \right)^2 + \frac{16}{3} \frac{\sigma^* \Upsilon_\infty^3}{\kappa^* \nu_f (\rho C_p)_f} \left( \frac{\partial \Upsilon}{\partial y} \right)^2 \right\} + \frac{\mu_{nf}}{\Upsilon_\infty} \left( \frac{\partial E_1}{\partial y} \right)^2 + \frac{\mu_{nf} u^2}{k \Upsilon_\infty}. \tag{21}$$

The non-dimensional entropy analysis formula can be described as [36]:

$$N_G = \frac{\Upsilon_\infty^2 b^2 E_G}{k_f (\Upsilon_w - \Upsilon_\infty)^2}. \tag{22}$$

By Equation (9), the non-dimensional entropy formula is:

$$N_G = R_\epsilon \left[ \phi_5 (1 + N_\epsilon) \theta'^2 + \frac{1}{\phi_1} \frac{B_\epsilon}{\Omega} \left( f''^2 + K_\epsilon f'^2 \right) \right], \tag{23}$$

Here,  $R_\epsilon$  is the Reynolds number,  $\Omega$  is the thermal gradient and  $B_\epsilon$  is the Brinkman number.

### 7. Results and Discussion

The succeeding conversation is given by numerical results reaching the model detailed in the prior portion. The possible parameters  $\bar{\omega}_1, \bar{\omega}_2, K_\epsilon, R_\epsilon, \phi, \Lambda_\epsilon, Y_\epsilon, N_\epsilon, Q_\epsilon, E_\epsilon, B_\gamma, S,$  and  $B_\epsilon$  are getting in this sector. These parameters display physical performance, such as velocity, energy, and entropy production, of the non-dimensional quantities in Figure 3a–c,

Figures 4, 5 and 6a,b. For Cu-EO and Ag-EO non-Newtonian P-ENFs, the consequences are gained. Table 4 details the skin friction coefficient and temperature differences. The defaulting values were  $\bar{\omega}_1 = 0.01$ ,  $\bar{\omega}_2 = 0.2$ ,  $K_\varepsilon = 0.6$ ,  $\phi = 0.1$ ,  $\Lambda_\varepsilon = 0.3$ ,  $Y_\varepsilon = 0.3$ ,  $N_\varepsilon = 0.3$ ,  $Q_\varepsilon = 0.1$ ,  $E_\varepsilon = 0.2$ ,  $B_{\gamma_r} = 0.3$ ,  $S = 0.5$ ,  $P_r = 6450$ ,  $R_\varepsilon = 5$  and  $B_\varepsilon = 5$ . The graphs in Figure 3a,b depict the flowing and thermal situation of two types of P-ENF with the combination of Cu-EO and Ag-EO concerning the influencing parameter  $\bar{\omega}_1$  over a stretched surface in PTSC. Fluidity and boundary layer thickness were decelerated to improve values of the Powell-Eyring parameter, which is responsible for increasing fluid viscosity to resist flow. Slower fluid takes longer to span the sheet, whereas passing fluid can absorb more heat. This is reflected in improved thermal distribution and the thermal boundary layer, increasing the Powell-Eyring metric [26]. The execution of the Cu-EO combination is remarked more effective than Ag-EO in the flowing fluid. Traces in Figure 3c highlight the entropy of the system raised concerning the impact of increment  $\bar{\omega}_1$  which correspondingly makes the heat transfer rate decrease. Table 4 shows that the relative share of the heat transfer rate increases as well. On point 25.0, it has also been found out that the relative minimum percentage of  $\bar{\omega}_1$  is reflected and when maximum reflected at point 28.1. By increasing the porosity of the medium used in the modeled PTSC, the porous media parameter ( $K_\varepsilon$ ) changes the physical condition in favor of flow speed and heat transfer. The graphical representations of Figure 4a,b demonstrated the assertion mentioned above that the Darcian force serves as a crucial element in such Ag-EO and Cu-EO combinations. In terms of thermal features of heat transfer rate as well as thermal boundary behavior, the preceding combination outperforms the other combination stated later, possibly because of its enhanced resistance to density rise for higher values of  $K_\varepsilon$  [39]. In these situations, the Cu-EO nanofluid seems more effective than the Ag-EO nanofluid. Drafts in Figure 4c disclosed the entropy rise concerning the improved permeability, leading to the heat transfer rate decrease. According to Table 4, increment in  $K_\varepsilon$  resulted in enhancing the relative percentage of heat transfer rate. 21.5 and 28.1 are minimum and maximum relative percentages of  $K_\varepsilon$ , respectively. Figure 5a,b shows the flow and thermal behavior of Ag-EO and Cu-EO-based flows across the stretched sheet as the nanoparticle fractional volume ( $\phi$ ) increases. This is a critical parameter in nanofluid research because the particle suspension has a proportionate ability to influence the physical properties of the fluid being studied. The increased  $\phi$  floating in the base fluid diminishes the flow of the fluid as well as the hydrodynamic boundary layer [26]. On the other hand, this slower velocity encourages temperature transport to raise the fluid temperature and thermal boundary layer for increasing solid volume fraction values. The positive entropy transitions for matching fractional volume increases are depicted in Figure 5c. Table 4 shows how the Nusselt number changes as the solid volume percentage increases. While  $\phi$  increment, the heat transfer rate of Cu-EO nanofluid appears to be somewhat more significant than that of Ag-EO nanofluid. Furthermore, it is also indicated in Table 4 that the smallest ratio of ( $\phi$ ) is reflected on point 24.0, and it is extreme on 28.1. Figure 6a,b reflects the boosted outcomes of irreversible energy loss in Cu-EO, and Ag-EO nanofluid flows for changing Reynolds Number  $R_\varepsilon$  and Brinkman Number ( $B_r$ ) respectively. As the  $Re$  increases, the dominant inertial force over the viscous force promotes the migration of nanoparticles through the medium's porous structure. This aids in the development of entropy over the domain region. Cu-EO nanofluid generated a higher entropy rate than Ag-EO nanofluid due to the combined efficiency of particles [25]. The heat created by the viscous features was modeled using the Brinkman number ( $B_\varepsilon$ ), which increased as the generated heat outweighed the thermal inputs from other factors. This increased viscosity, along with its increased heat-inducing capabilities, enhances total entropy development ( $N_G$ ). Elevated entropy layers for increasing Brinkman number  $B_\varepsilon$  values can be indicative of the process as mentioned earlier in Figure 6b.

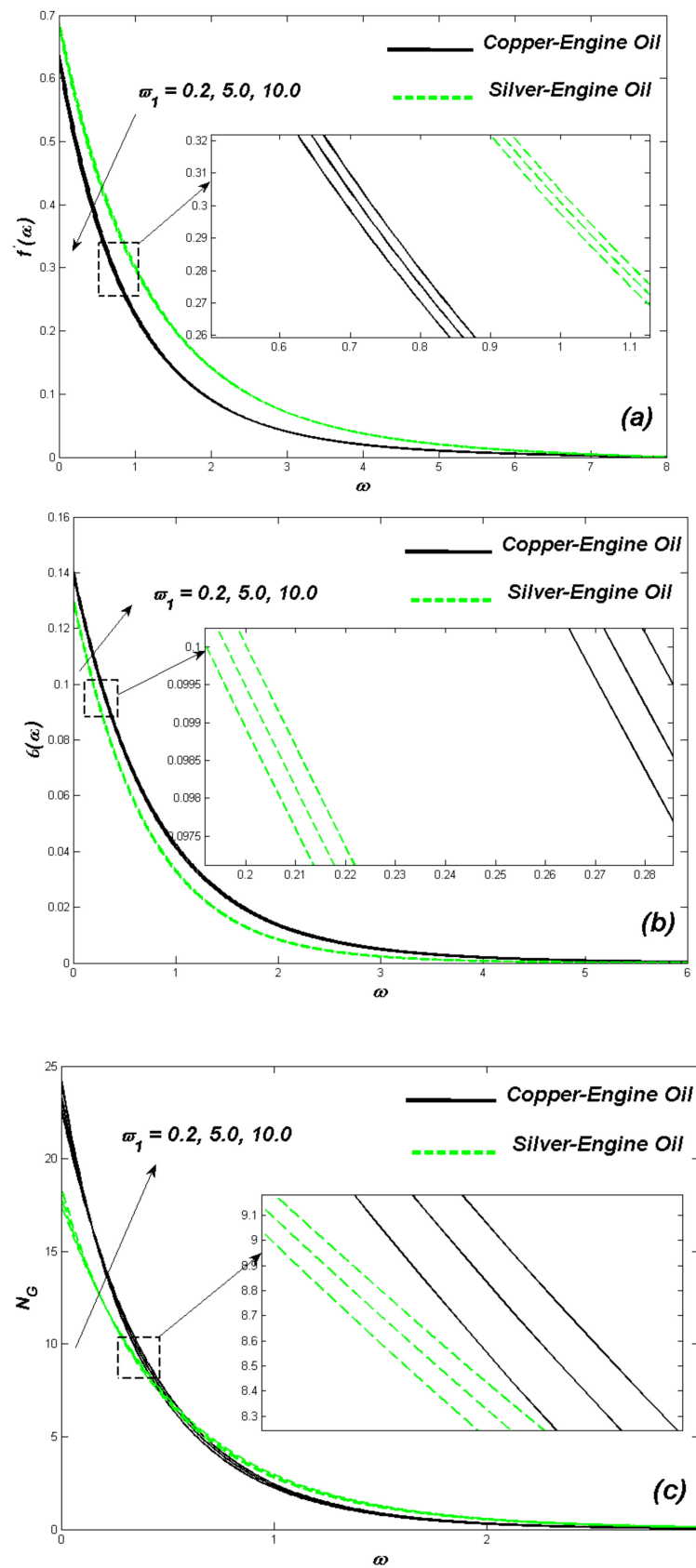


Figure 3. (a) Velocity change with  $\bar{\omega}_1$ . (b) Temperature change with  $\bar{\omega}_1$ . (c) Entropy change with  $\bar{\omega}_1$ .

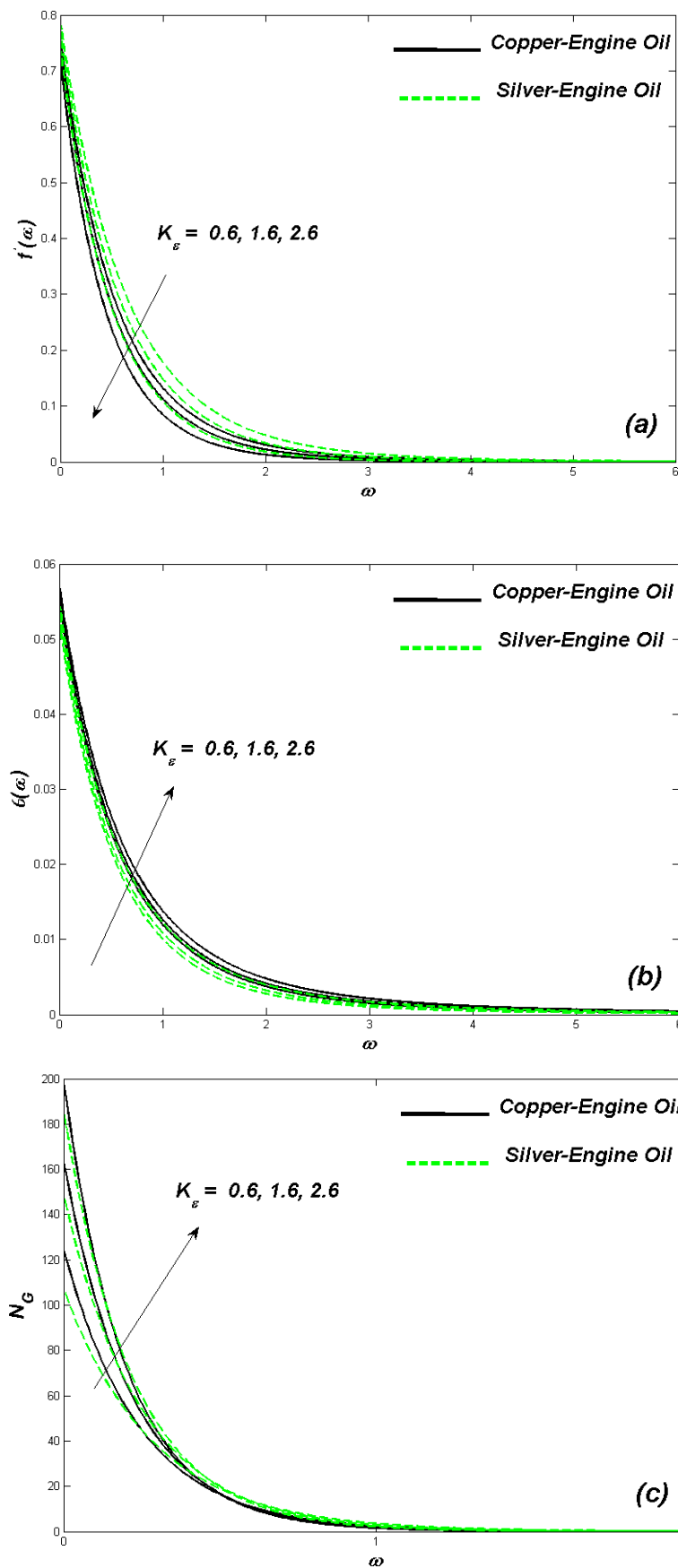


Figure 4. (a) Velocity change with  $K_\epsilon$ . (b) Temperature change with  $K_\epsilon$ . (c) Entropy change with  $K_\epsilon$ .

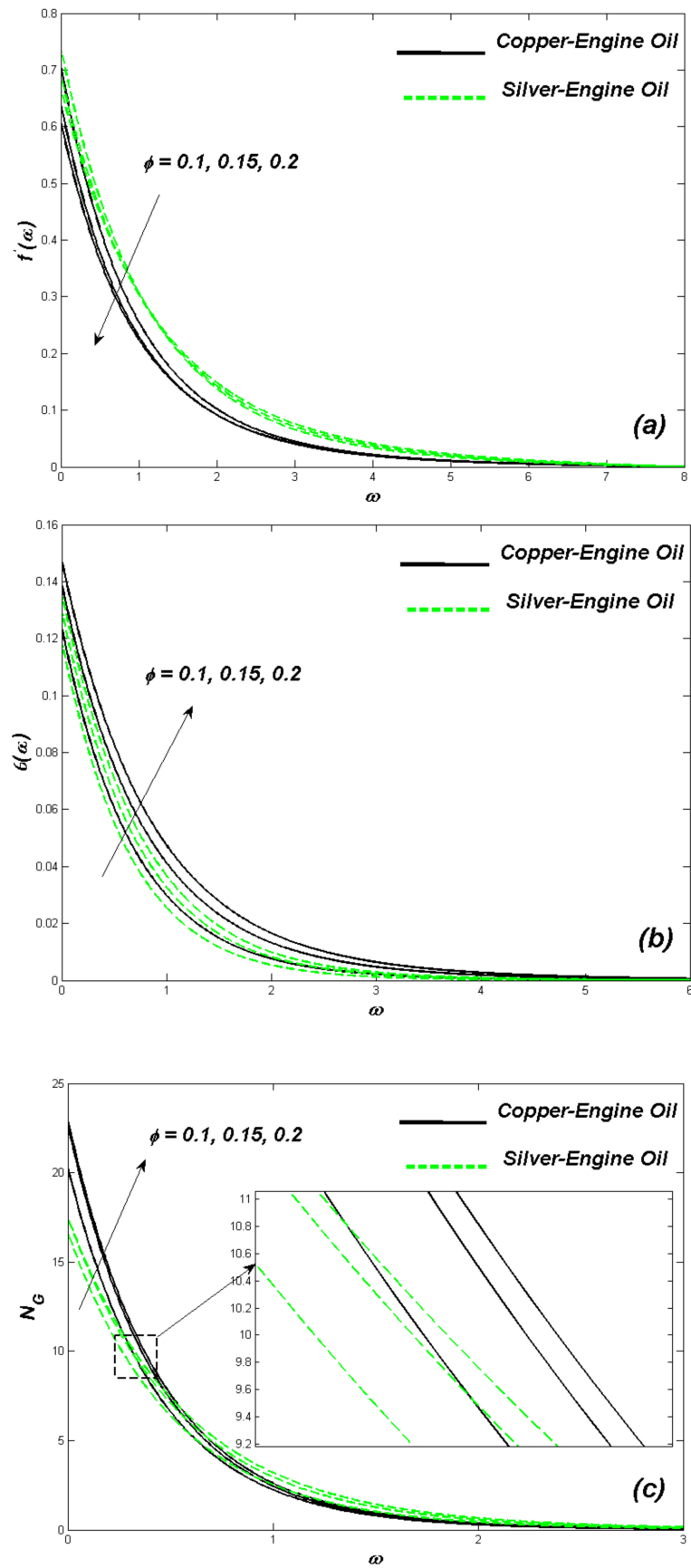


Figure 5. (a) Velocity change with  $\phi$ . (b) Temperature change with  $\phi$ . (c) Entropy change with  $\phi$ .

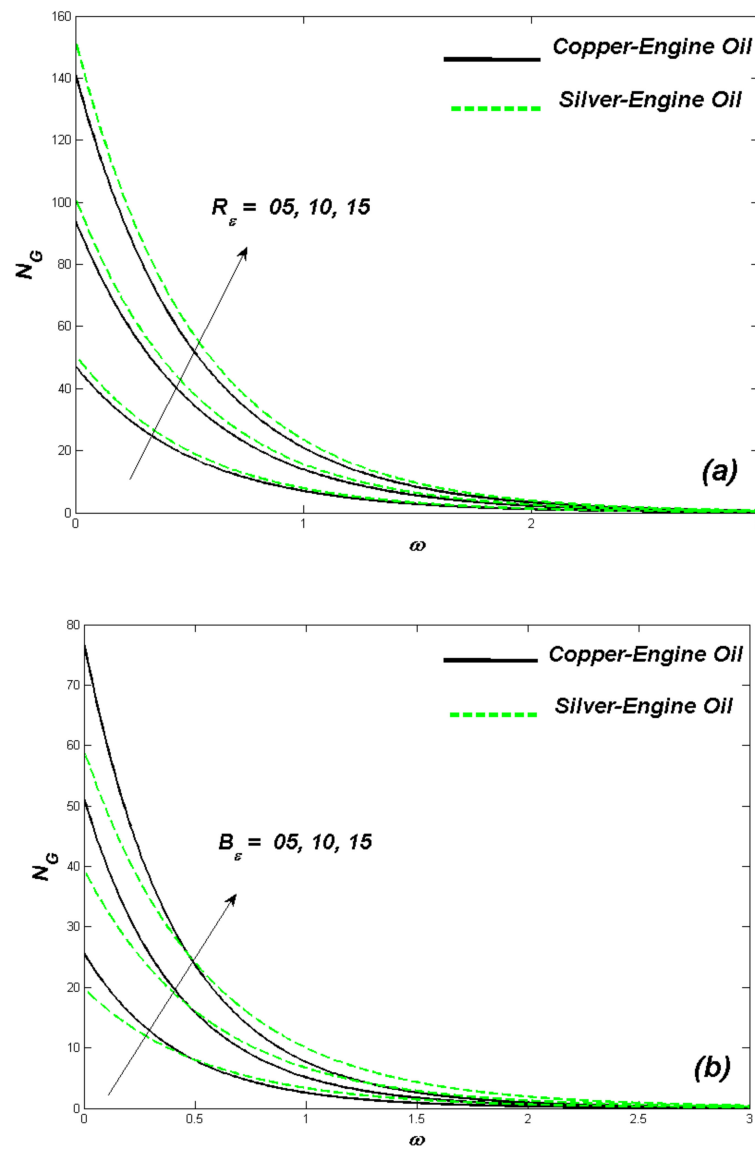


Figure 6. (a). Velocity change with  $R_\epsilon$ . (b) Temperature change with  $B_\epsilon$ .

Table 4. Skin friction ( $C_f Re_x^{\frac{1}{2}}$ ) and Nusselt Number ( $N_u Re_x^{-\frac{1}{2}}$ ) values for  $Pr = 6450$ .

$\bar{\omega}_1$	$\bar{\omega}_2$	$K_\epsilon$	$\phi$	$\Lambda_\epsilon$	$Y_\epsilon$	$S$	$N_\epsilon$	$E_\epsilon$	$B_\gamma$	$C_f Re_x^{\frac{1}{2}}$	$C_f Re_x^{\frac{1}{2}}$	$N_u Re_x^{-\frac{1}{2}}$	$N_u Re_x^{-\frac{1}{2}}$	$\frac{N_u(Cu) - N_u(Ag)}{N_u(Cu)} \times 100$	
										Cu-EO	Ag-EO	Cu-EO	Ag-EO		
0.2 5.0 10	0.5	0.6	0.1	0.3	0.3	0.5	0.3	0.2	0.3	2.6840	2.4015	0.1951	0.1402	28.1%	
										2.7051	2.4251	0.1728	0.1245	27.9%	
										2.7405	2.4530	0.1531	0.1147	25.0%	
										2.7461	2.4429	0.1512	0.0933	38.2%	
										2.7295	2.4263	0.1724	0.1202	30.2%	
										2.6840	2.4015	0.1951	0.1402	28.1%	
	0.1 0.3 0.5	0.6	1.6	0.1	0.3	0.3	0.5	0.3	0.2	0.3	2.6840	2.4015	0.1951	0.1402	28.1%
											2.7112	2.4327	0.1723	0.1270	26.2%
											2.7554	2.4736	0.1324	0.1039	21.5%
											2.6840	2.4015	0.1951	0.1402	28.1%
											2.7144	2.4215	0.2113	0.1546	26.8%
											2.7461	2.4529	0.2412	0.1833	24.0%
	0.15 0.2	1.6	2.6	0.1	0.3	0.3	0.5	0.3	0.2	0.3	2.7431	2.4554	0.2428	0.1979	18.4%
											2.7105	2.4238	0.2156	0.1646	23.6%
											2.6840	2.4015	0.1951	0.1402	28.1%
											2.6840	2.4015	0.1513	0.0979	35.2%
											2.6840	2.4015	0.1756	0.1246	29.0%
											2.6840	2.4015	0.1951	0.1402	28.1%

Table 4. Cont.

$\bar{\omega}_1$	$\bar{\omega}_2$	$K_\epsilon$	$\phi$	$\Lambda_\epsilon$	$Y_\epsilon$	$S$	$N_\epsilon$	$E_\epsilon$	$B_\gamma$	$C_f Re_x^{\frac{1}{2}}$ Cu-EO	$C_f Re_x^{\frac{1}{2}}$ Ag-EO	$Nu Re_x^{-\frac{1}{2}}$ Cu-EO	$Nu Re_x^{-\frac{1}{2}}$ Ag-EO	$\frac{Nu_{(Cu)} - Nu_{(Ag)}}{Nu_{(Cu)}} \times 100$
						0.3				2.6530	2.3837	0.1784	0.1217	31.7%
						0.5				2.6840	2.4015	0.1951	0.1402	28.1%
						0.7				2.7146	2.4414	0.2288	0.1702	25.6%
							0.1			2.6840	2.4015	0.1823	0.1286	29.4%
							0.3			2.6840	2.4015	0.1951	0.1402	28.1%
							0.5			2.6840	2.4015	0.2216	0.1745	21.2%
								0.1		2.6840	2.4015	0.1843	0.1233	33.0%
								0.2		2.6840	2.4015	0.1951	0.1402	28.1%
								0.4		2.6840	2.4015	0.2049	0.1741	15.0%
									0.1	2.6840	2.4015	0.2109	0.1739	17.5%
									0.3	2.6840	2.4015	0.1951	0.1402	28.1%
									0.5	2.6840	2.4015	0.1787	0.1142	36.0%

### 8. Conclusions

This study conducted a numerical investigation of boundary layer flow for Ag and Cu-engine oil nanoliquids over a porous stretching sheet in PTSC. The survey considered a porous media, heat source, viscous dissipation, thermal radiation, and Cattaneo–Christov heat flux. Graphical plots disclose the outcomes of the work engaging the Keller-Box method for solution. The following conclusive outcomes were derived from the above results:

1. By raising nano fractional volume parameter  $\phi$  and Powell-Eyring metric  $\zeta$ , a deceleration in the velocity is noted.
2. An enhancement in the thermal distribution for the set of metrics  $\bar{\omega}_1, K_\epsilon, \phi, E_\epsilon, B_\gamma, Nu$  is seen whereas it gets reduced for an increase in the parameter  $Y_\epsilon$ .
3. The parameters have exciting impacts on the heat transfer rate near the wall and become negligible as it moves further away from it.
4. The thermal performance of Cu-EO over Ag-EO held at a minimal rate of 15.0% and maximized up to 36.0%.
5. The study reveals an increase in system entropy on the increase in Reynolds number, Brinkmann number, Eckert number, and reduced velocity slip parameter  $\Lambda$  increment.
6. For the same amount of nanoparticles, it is achieved that the Cu-EO nanofluid is a better heat transporter agent than the Ag-EO nanofluid.

**Author Contributions:** Conceptualization, M.R.S., N.H.A.-H., M.G.; methodology, R.A.A., N.H.A.-H.; software, M.A.A.; validation, M.A.A.; investigation, R.A.A.; resources, M.A.A.; visualization, N.H.A.-H.; data curation, M.J.H.R.; writing—original draft preparation, M.G., M.R.S.; writing—review and editing, M.J.H.R.; supervision, M.G., M.R.S.; project administration, M.G., N.H.A.-H.; funding acquisition, M.R.S., N.H.A.-H. All authors have read and agreed to the published version of the manuscript.

**Funding:** This research work was funded by Institutional Fund Projects under grant no. (IFPNC-006-135-2020). Therefore, the authors gratefully acknowledge technical and financial support from the Ministry of Education and King Abdulaziz University, Jeddah, Saudi Arabia.

**Institutional Review Board Statement:** Not applicable.

**Informed Consent Statement:** Not applicable.

**Data Availability Statement:** Not applicable.

**Acknowledgments:** The great help from King Abdulaziz University’s faculty members, including Abdulmalik A. Aljinaidi, Mohamed A. Eltaher, Khalid H. Almitani, Khaled A. Alnefaie, Abdullah M. Abusorrah, and Hatem F. Sindi are really appreciated.

**Conflicts of Interest:** The authors declare no conflict of interest.

## Nomenclatures

$b$	initial stretching rate
$B_\gamma$	Biot number
$B_\varepsilon$	Brinkman number
$C_f$	Drag force
$C_p$	Specific heat ( $\text{J kg}^{-1} \text{K}^{-1}$ )
$E_\varepsilon$	Eckert number
$E_G$	entropy (J/K)
$h_L$	heat transfer coefficient
$k$	fluid porosity
$\kappa$	thermal conductivity ( $\text{W m}^{-1} \text{K}^{-1}$ )
$k_L$	surface thermal conductivity
$k^*$	absorption coefficient
$K_\varepsilon$	porous media parameter
$N_\xi$	radiation parameter
$N_G$	dimensionless entropy generation
$Nu_x$	local Nusselt number
$Pr$	Prandtl number ( $\nu/\alpha$ )
$q$	column vectors of order $J \times 1$
$q_r$	radiative heat flux
$q_w$	wall heat flux
$Re$	Reynolds number
$S$	suction/injection parameter
$E_1, E_2$	velocity component in $x, y$ direction ( $\text{m s}^{-1}$ )
$U_w$	velocity of the stretching sheet
$V_L$	vertical velocity
$x, y$	dimensional space coordinates (m)

### Greek Symbols

$\Upsilon$	fluid temperature
$\Upsilon_w$	surface fluid temperature
$\Upsilon_\infty$	ambient temperature
$\phi$	volume fraction of the nanoparticles
$\rho$	density ( $\text{kg m}^{-3}$ )
$\sigma^*$	Stefan-Boltzmann constant
$\psi$	stream function
$\omega$	independent similarity variable
$\theta$	dimensionless temperature
$\bar{\omega}_1$	Powell-Eyring parameter-I
$\bar{\omega}_2$	Powell-Eyring parameter-II
$Y$	relaxation time
$\Lambda_\varepsilon$	velocity slip parameter
$\mu$	dynamic viscosity of the fluid ( $\text{kg m}^{-1} \text{s}^{-1}$ )
$\nu$	kinematic viscosity of the fluid ( $\text{m}^2 \text{s}^{-1}$ )
$\alpha$	thermal diffusivity ( $\text{m}^2 \text{s}^{-1}$ )
$\Omega$	dimensionless temperature gradient

### Subscripts

$f$	base fluid
$nf$	nanofluid
$s$	particles

## References

1. Olia, H.; Torabi, M.; Bahiraei, M.; Ahmadi, M.H.; Goodarzi, M.; Safaei, M.R. Application of Nanofluids in Thermal Performance Enhancement of Parabolic Trough Solar Collector: State-of-the-Art. *Appl. Sci.* **2019**, *9*, 463. [[CrossRef](#)]
2. Masoud Hosseini, S.; Safaei, M.R.; Estellé, P.; Hadi Jafarnia, S. Heat transfer of water-based carbon nanotube nanofluids in the shell and tube cooling heat exchangers of the gasoline product of the residue fluid catalytic cracking unit. *J. Therm. Anal. Calorim.* **2020**, *140*, 351–362. [[CrossRef](#)]

3. Safaei, M.R.; Tlili, I.; Gholamalizadeh, E.; Abbas, T.; Alkanhal, T.A.; Goodarzi, M.; Dahari, M. Thermal analysis of a binary base fluid in pool boiling system of glycol–water alumina nano-suspension. *J. Therm. Anal. Calorim.* **2021**, *143*, 2453–2462. [[CrossRef](#)]
4. Bahiraei, M.; Salmi, H.K.; Safaei, M.R. Effect of employing a new biological nanofluid containing functionalized graphene nanoplatelets on thermal and hydraulic characteristics of a spiral heat exchanger. *Energy Convers. Manag.* **2019**, *180*, 72–82. [[CrossRef](#)]
5. Hosseini, S.M.; Safaei, M.R.; Goodarzi, M.; Alrashed, A.A.; Nguyen, T.K. New temperature, interfacial shell dependent dimensionless model for thermal conductivity of nanofluids. *Int. J. Heat Mass Transf.* **2017**, *114*, 207–210. [[CrossRef](#)]
6. Gheynani, A.R.; Akbari, O.A.; Zarringhalam, M.; Shabani, G.A.S.; Alnaqi, A.A.; Goodarzi, M.; Toghraie, D. Investigating the effect of nanoparticles diameter on turbulent flow and heat transfer properties of non-Newtonian carboxymethyl cellulose/CuO fluid in a microtube. *Int. J. Numer. Methods Heat Fluid Flow* **2019**, *29*, 1699–1723. [[CrossRef](#)]
7. Goodarzi, M.; Javid, S.; Sajadifar, A.; Nojoomizadeh, M.; Motaharipour, S.H.; Bach, Q.-V.; Karimipour, A. Slip velocity and temperature jump of a non-Newtonian nanofluid, aqueous solution of carboxy-methyl cellulose/aluminum oxide nanoparticles, through a microtube. *Int. J. Numer. Methods Heat Fluid Flow* **2019**, *29*, 1606–1628. [[CrossRef](#)]
8. Ellahi, R.; Hussain, F.; Abbas, S.A.; Sarafraz, M.M.; Goodarzi, M.; Shadloo, M.S. Study of Two-Phase Newtonian Nanofluid Flow Hybrid with Hafnium Particles under the Effects of Slip. *Inventions* **2020**, *5*, 6. [[CrossRef](#)]
9. Powell, R.E.; Eyring, H. Mechanisms for the Relaxation Theory of Viscosity. *Nat. Cell Biol.* **1944**, *154*, 427–428. [[CrossRef](#)]
10. Muhammad, T.; Waqas, H.; Khan, S.A.; Ellahi, R.; Sait, S.M. Significance of nonlinear thermal radiation in 3D Eyring–Powell nanofluid flow with Arrhenius activation energy. *J. Therm. Anal. Calorim.* **2021**, *143*, 929–944. [[CrossRef](#)]
11. Hayat, T.; Iqbal, Z.; Qasim, M.; Obaidat, S. Steady flow of an Eyring Powell fluid over a moving surface with convective boundary conditions. *Int. J. Heat Mass Transf.* **2012**, *55*, 1817–1822. [[CrossRef](#)]
12. Jamshed, W.; Eid, M.R.; Nasir, N.A.A.M.; Nisar, K.S.; Aziz, A.; Shahzad, F.; Saleel, C.A.; Shukla, A. Thermal examination of renewable solar energy in parabolic trough solar collector utilizing Maxwell nanofluid: A noble case study. *Case Stud. Therm. Eng.* **2021**, *27*, 101258. [[CrossRef](#)]
13. Sajid, T.; Jamshed, W.; Shahzad, F.; Eid, M.R.; Akgül, E.K.; Nisar, K.S. Entropy Analysis and Thermal Characteristics of Reiner Philippoff Hybrid Nanofluidic Flow Via a Parabolic Trough of Solar Aircraft Wings: Keller Box Method. *Res. Sq.* **2021**, Preprints. [[CrossRef](#)]
14. Al-Rashed, A.A.; Alnaqi, A.A.; Alsarraf, J. Numerical investigation and neural network modeling of the performance of a dual-fluid parabolic trough solar collector containing non-Newtonian water-CMC/Al<sub>2</sub>O<sub>3</sub> nanofluid. *Sustain. Energy Technol. Assess.* **2021**, *48*, 101555. [[CrossRef](#)]
15. Mwesigye, A.; Yilmaz, I.H.; Meyer, J.P. Numerical analysis of the thermal and thermodynamic performance of a parabolic trough solar collector using SWCNTs-Therminol®VP-1 nanofluid. *Renew. Energy* **2018**, *119*, 844–862. [[CrossRef](#)]
16. Siavashi, M.; Bozorg, M.V.; Toosi, M.H. A numerical analysis of the effects of nanofluid and porous media utilization on the performance of parabolic trough solar collectors. *Sustain. Energy Technol. Assess.* **2021**, *45*, 101179. [[CrossRef](#)]
17. Xiong, Q.; Bozorg, M.V.; Doranehgard, M.H.; Hong, K.; Lorenzini, G. A CFD investigation of the effect of non-Newtonian behavior of Cu–water nanofluids on their heat transfer and flow friction characteristics. *J. Therm. Anal. Calorim.* **2020**, *139*, 2601–2621. [[CrossRef](#)]
18. Ebrahimi-Moghadam, A.; Mohseni-Gharyehsafa, B.; Farzaneh-Gord, M. Using artificial neural network and quadratic algorithm for minimizing entropy generation of Al<sub>2</sub>O<sub>3</sub>-EG/W nanofluid flow inside parabolic trough solar collector. *Renew. Energy* **2018**, *129*, 473–485. [[CrossRef](#)]
19. Yan, S.-R.; Golzar, A.; Sharifpur, M.; Meyer, J.P.; Liu, D.-H.; Afrand, M. Effect of U-shaped absorber tube on thermal-hydraulic performance and efficiency of two-fluid parabolic solar collector containing two-phase hybrid non-Newtonian nanofluids. *Int. J. Mech. Sci.* **2020**, *185*, 105832. [[CrossRef](#)]
20. Chaudhari, K.; Walke, P.; Wankhede, U.; Shelke, R. An Experimental Investigation of a Nanofluid (Al<sub>2</sub>O<sub>3</sub> + H<sub>2</sub>O) Based Parabolic Trough Solar Collectors. *Br. J. Appl. Sci. Technol.* **2015**, *9*, 551–557. [[CrossRef](#)]
21. Okonkwo, E.C.; Adun, H.; Babatunde, A.; Abid, M.; Ratlamwala, T.A. Entropy Generation Minimization in a Parabolic Trough Collector Operating with SiO<sub>2</sub>–Water Nanofluids Using the Genetic Algorithm and Artificial Neural Network. *J. Therm. Sci. Eng. Appl.* **2019**, *12*, 031007. [[CrossRef](#)]
22. Okonkwo, E.C.; Abid, M.; Ratlamwala, T.A.H.; Abbasoglu, S.; Dagbasi, M. Optimal Analysis of Entropy Generation and Heat Transfer in Parabolic Trough Collector Using Green-Synthesized TiO<sub>2</sub>/Water Nanofluids. *J. Sol. Energy Eng.* **2019**, *141*, 031011. [[CrossRef](#)]
23. Hachicha, A.A.; Said, Z.; Rahman, S.; Al-Sarairah, E. On the thermal and thermodynamic analysis of parabolic trough collector technology using industrial-grade MWCNT based nanofluid. *Renew. Energy* **2020**, *161*, 1303–1317. [[CrossRef](#)]
24. Jamshed, W.; Nisar, K.S.; Ibrahim, R.W.; Shahzad, F.; Eid, M.R. Thermal expansion optimization in solar aircraft using tangent hyperbolic hybrid nanofluid: A solar thermal application. *J. Mater. Res. Technol.* **2021**, *14*, 985–1006. [[CrossRef](#)]
25. Jamshed, W.; Akgül, E.K.; Nisar, K.S. Keller box study for inclined magnetically driven Casson nanofluid over a stretching sheet: Single phase model. *Phys. Scr.* **2021**, *96*, 065201. [[CrossRef](#)]
26. Jamshed, W.; Aziz, A. A comparative entropy based analysis of Cu and Fe<sub>3</sub>O<sub>4</sub>/methanol Powell-Eyring nanofluid in solar thermal collectors subjected to thermal radiation, variable thermal conductivity and impact of different nanoparticles shape. *Results Phys.* **2018**, *9*, 195–205. [[CrossRef](#)]

27. Jamshed, W.; Nisar, K.S. Computational single-phase comparative study of a Williamson nanofluid in a parabolic trough solar collector via the Keller box method. *Int. J. Energy Res.* **2021**, *45*, 10696–10718. [[CrossRef](#)]
28. Aziz, A.; Jamshed, W.; Aziz, T.; Bahaidarah, H.M.S.; Rehman, K.U. Entropy analysis of Powell–Eyring hybrid nanofluid including effect of linear thermal radiation and viscous dissipation. *J. Therm. Anal. Calorim.* **2021**, *143*, 1331–1343. [[CrossRef](#)]
29. Goodarzi, M.; Safaei, M.R.; Vafai, K.; Ahmadi, G.; Dahari, M.; Kazi, S.; Jomhari, N. Investigation of nanofluid mixed convection in a shallow cavity using a two-phase mixture model. *Int. J. Therm. Sci.* **2014**, *75*, 204–220. [[CrossRef](#)]
30. Ebrahimi, D.; Yousefzadeh, S.; Akbari, O.A.; Montazerifar, F.; Rozati, S.A.; Nakhjavani, S.; Safaei, M.R. Mixed convection heat transfer of a nanofluid in a closed elbow-shaped cavity (CESC). *J. Therm. Anal. Calorim.* **2021**, *144*, 2295–2316. [[CrossRef](#)]
31. Brewster, M.Q. *Thermal Radiative Transfer and Properties*; John Wiley & Sons: New York, NY, USA, 1992.
32. Iqbal, Z.; Azhar, E.; Maraj, E. Performance of nano-powders SiO<sub>2</sub> and SiC in the flow of engine oil over a rotating disk influenced by thermal jump conditions. *Phys. A Stat. Mech. Appl.* **2021**, *565*, 125570. [[CrossRef](#)]
33. Karimipour, A.; Esfe, M.H.; Safaei, M.R.; Semiromi, D.T.; Jafari, S.; Kazi, S. Mixed convection of copper–water nanofluid in a shallow inclined lid driven cavity using the lattice Boltzmann method. *Phys. A Stat. Mech. Appl.* **2014**, *402*, 150–168. [[CrossRef](#)]
34. Alipour, H.; Karimipour, A.; Safaei, M.R.; Semiromi, D.T.; Akbari, O.A. Influence of T-semi attached rib on turbulent flow and heat transfer parameters of a silver-water nanofluid with different volume fractions in a three-dimensional trapezoidal microchannel. *Phys. E Low-Dimens. Syst. Nanostruct.* **2017**, *88*, 60–76. [[CrossRef](#)]
35. Keller, H.B. A new difference scheme for parabolic problems. In *Numerical Solution of Partial Differential Equations–II.*; Elsevier: Amsterdam, The Netherlands, 1971; pp. 327–350.
36. Jamshed, W.; Nisar, K.S.; Ibrahim, R.W.; Mukhtar, T.; Vijayakumar, V.; Ahmed, F. Computational frame work of Cattaneo-Christov heat flux effects on Engine Oil based Williamson hybrid nanofluids: A thermal case study. *Case Stud. Therm. Eng.* **2021**, *26*, 101179. [[CrossRef](#)]
37. Rana, S.; Nawaz, M. Investigation of enhancement of heat transfer in Sutterby nanofluid using Koo–Kleinstreuer and Li (KKL) correlations and Cattaneo–Christov heat flux model. *Phys. Scr.* **2019**, *94*, 115213. [[CrossRef](#)]
38. Das, S.; Chakraborty, S.P.; Jana, R.N.; Makinde, O.D. Entropy analysis of unsteady magneto-nanofluid flow past accelerating stretching sheet with convective boundary condition. *Appl. Math. Mech.* **2015**, *36*, 1593–1610. [[CrossRef](#)]
39. Aziz, A.; Jamshed, W.; Aziz, T. Mathematical model for thermal and entropy analysis of thermal solar collectors by using Maxwell nanofluids with slip conditions, thermal radiation and variable thermal conductivity. *Open Phys.* **2018**, *16*, 123–136. [[CrossRef](#)]